Wave propagation in two-dimensional viscoelastic metamaterials

Yan-Feng Wang,[1] Yue-Sheng Wang,[1,*] and Vincent Laude[2,†]

[1]*Institute of Engineering Mechanics, Beijing Jiaotong University, Beijing 100044, People's Republic of China*

[2]*Franche-Comté Electronique Mécanique Thermique et Optique, CNRS UMR 6174, Université de Franche-Comté, 25030 Besancon, France*

(Received 6 June 2015; revised manuscript received 8 September 2015; published 30 September 2015)

Propagation of elastic waves in acoustic metamaterials based on locally resonant viscoelastic phononic crystals is discussed. A variational formulation of the complex band structure for in-plane polarized waves is proposed and used to formulate a finite element model. Two different types of locally resonant band gaps are found for quasilongitudinal and quasishear waves, with distinct features in terms of complex bands and transmission bandwidth. The influence of viscosity on the complex band structure, transmission properties, and effective dynamic mass density of two-dimensional locally resonant metamaterials is further investigated. It is found that bands that were degenerate in the elastic case are separated when viscosity is introduced, and that sharp corners at high symmetry points become rounded. Transmission is generally worsened in passing bands, while it is enhanced inside locally resonant band gaps, contrary to what was observed previously for Bragg band gaps. All changes in the complex band structure and transmission spectra are solely due to the dispersive and dissipative effects of viscosity. It is also found that the negative mass density property may also disappear when viscosity is introduced. These results are relevant to practical applications of elastic and viscoelastic metamaterials.

DOI: 10.1103/PhysRevB.92.104110 PACS number(s): 62.20.D−, 63.20.D−, 46.35.+z, 62.40.+i

I. INTRODUCTION

The study of elastic wave propagation in periodic composite materials or structures has attracted a growing interest in recent years. Phononic crystal (PC) [1], which may induce band gaps, is a kind of periodic composite containing two or more component materials with different elastic constants and mass densities. The phononic band gap is a frequency range within which all propagating Bloch waves are prohibited regardless of their wave vector and polarization. Major mechanisms that can generate band gaps are Bragg scattering [1] and local resonance [2]. The presence of a local resonance is a key feature of acoustic/elastic metamaterials (which exhibit properties generally going beyond what we expect to find in natural or conventional materials), with potential application in the reduction of noise and vibration at low frequencies [3].

Numerous studies have explored the properties of PCs and metamaterials. Nonetheless, most reported theoretical works consider systems with elastic (undamped) constituents, within which waves can propagate without attenuation on propagation. Ideal materials of this kind do not exist in nature, although weakly damped materials are often approximated in this manner. In actual experiments, one or more constitutive materials can present both elastic and viscous properties. The famous quote of Heraclit, "All entities move and nothing remains still," indeed implies that everything has viscosity. In other words, the constituents may be viscoelastic in the frequency range of interest. The presence of viscosity results in temporal damping or spatial attenuation of waves as they freely propagate through the periodic medium [4]. Taking viscosity into account may obviously lead to changes in band structures as well as in transmission spectra.

Although several viscoelastic models have been used to describe propagation losses, material loss has not been extensively considered in the various theories of PCs [4]. The existing studies can be generally classified into the following two different types.

First, some studies were concerned with the transmission properties of finite structures. Merheb *et al.* [5] studied the effect of viscoelasticity on the transmission properties of rubber/air PCs under the standard linear solid model by using a finite difference time domain (FDTD) method. Psarobas [6] theoretically obtained the transmission spectrum of a three-dimensional (3D) sonic crystal composed of viscoelastic rubber spheres in air with the Kelvin-Voigt model. By using the FDTD method in conjunction with a Kelvin-Voigt model with fractional derivatives, Liu *et al.* [7] examined 2D PCs constituting of aluminum cylinders in a rubber matrix. In their model, viscosity in rubber was limited to low frequencies. Oh *et al.* [8] investigated wave attenuation and dissipation mechanisms in viscoelastic PCs with inclusions of different material types.

Second, infinite periodic crystals have been described by the transformation of their band structure. Research in this area can be divided into two categories [3]: either free wave propagation which is usually associated with impulsive loading, or time-harmonic wave propagation which is useful for comparison with experiments on long PC systems subjected to forced harmonic loading.

Free wave propagation only considers a real wave number k (or only propagating modes), and the frequency is allowed to become complex, $\omega = \omega' + i\omega''$, where the imaginary part ω'' measures damping of the mode in time. Mukherjee and Lee [9] studied the dispersion relations of laminated solid/fluid composites by using finite difference methods back in 1975, where the fluid was considered to be viscoelastic. Sprik and Wegdam [10], and Zhang *et al.* [11] investigated the complex bands of similar systems with three- or two-dimensional periodicity by using the plane wave expansion (PWE) method. Zhao and Wei discussed the effects of the viscoelasticity on the band gaps of one- [12] or two-dimensional [13] solid/solid PCs by using the PWE method. The effect of Rayleigh damping on

*Corresponding author: yswang@bjtu.edu.cn

†Corresponding author: vincent.laude@femto-st.fr

the band structure of solid/solid systems was also studied by Hussein [14] and co-authors [15].

In this paper, we consider time-harmonic wave propagation, a physically more realistic case [16], arguably, where a forcing frequency is taken as the real independent variable and the solution of the propagation problem results in a complex wave number describing the spatially attenuated Bloch wave [17]. The complex band structure is then obtained, where the real part and the imaginary part of the wave vector are presented separately. Sprik and Wegdam [10] studied the effects of a viscous fluid on the complex bands of the one-dimensional solid/fluid system. Moiseyenko *et al.* [18] investigated the influence of material loss on the complex band structure and group velocity in PCs assuming viscosity increasing linearly with frequency. The extended plane wave expansion (EPWE) method was used in this case, and only pure shear wave propagation was considered. Collet *et al.* [19] illustrated the complex band structure of a 2D damped PC slab with stubbed surfaces by using variational formulations. A theoretical analysis was carried out by Laude *et al.* [20] to investigate the transformation of the complex band structure of photonic and phononic crystals under the influence of loss. Andreassen and Jensen [21] compared the complex band structures for free and time-harmonic wave propagation, and found that those were in good agreement for small to medium amounts of material dissipation and for long wavelengths.

Moreover, the basic mechanism of local resonance inside metamaterials can give rise to material properties that are outside the realm provided by Nature at long wavelengths, such as negative mass density (NMD) related to a dipolar resonance [2]. Various metamaterials with different components, i.e., fluid/solid systems [22–27] and solid systems with different phases [26–31], were designed and investigated in this respect. Lattice systems with masses and springs [32–34] were also used to construct simplified models to illustrate the physical mechanism of the negative properties of metamaterials. However, for almost all reported metamaterials, viscosity is not taken into account when calculating the effective mass density.

In this paper, we study the complex band structure and the transmission properties of a 2D viscoelastic metamaterial composed of circular metal bars coated with rubber and periodically embedded in a polymer matrix. Either the coating or the matrix is considered viscoelastic. An algorithm for calculating the complex band structure for in-plane polarized waves is developed based on a finite element method (FEM). The effect of viscosity on the complex band structure [35] is discussed for the viscoelastic metamaterial. The transmission through a finite viscoelastic metamaterial is also calculated. The effective mass density of the viscoelastic metamaterial is used to explain some of the observed features.

II. MODELS AND FORMULATIONS

For linearly viscoelastic materials, loads and deformations are linearly related. The deformation depends not only on the present magnitude of the loads but also on the history of the loading process. The constitutive equations are thus different from those of elastic materials. The general relation between the components of the stress and strain tensors for an anisotropic and linear viscoelastic medium is given by [36]

$$T_I(\mathbf{r},t) = \dot{\psi}_{IJ}(t) * S_J(\mathbf{r},t), \tag{1}$$

where t is the time variable, $\mathbf{r}$ is the position vector, the asterisk ($*$) indicates time convolution, and ψ_{IJ} are the 21 independent components of the relaxation function with indices $I,J = 1,2,3,4,5,6$ satisfying the following relationship [37]:

$$\begin{aligned} &1 \leftrightarrow xx, \quad 2 \leftrightarrow yy, \quad 3 \leftrightarrow zz, \quad 4 \leftrightarrow yz,zy, \\ &5 \leftrightarrow xz,zx, \quad 6 \leftrightarrow xy,yx, \end{aligned} \tag{2}$$

$$\mathbf{T} = [\sigma_{xx},\sigma_{yy},\sigma_{zz},\sigma_{yz},\sigma_{xz},\sigma_{xy}]^{\mathrm{T}}, \text{ and}$$

$$\mathbf{S} = [\varepsilon_{xx},\varepsilon_{yy},\varepsilon_{zz},\varepsilon_{yz},\varepsilon_{xz},\varepsilon_{xy}]^{\mathrm{T}} \tag{3}$$

are the stress and the strain vectors written in contracted forms, respectively. For a time-harmonic plane wave with angular frequency ω propagating in the viscoelastic medium, a general solution for the displacement is of the form

$$u_j(\mathbf{r},t) = \tilde{u}_j(\mathbf{r})e^{i\omega t}, \tag{4}$$

with $i = \sqrt{-1}$, $j = 1,2,3$, and $\tilde{\mathbf{u}}_j(\mathbf{r})$ being a function of the position, independent of time. The stress and the strain vectors also have a similar form,

$$T_j(\mathbf{r},t) = \tilde{T}_j e^{i\omega t} \text{ and } S_j(\mathbf{r},t) = \tilde{S}_j e^{i\omega t}. \tag{5}$$

The constitutive relation in Eq. (1) can then be rewritten as

$$\tilde{\mathbf{T}} = \mathbf{C}^v(i\omega) \cdot \tilde{\mathbf{S}}, \tag{6}$$

where the components of the complex stiffness matrix $\mathbf{C}^v$ are

$$C^v_{IJ}(i\omega) = \int_{-\infty}^{\infty} \dot{\psi}_{IJ}(t)e^{-i\omega t}dt. \tag{7}$$

In this paper, either the coating or the matrix can be viscoelastic. Viscosity is assumed to increase linearly with frequency as is proper to polymers. The complex stiffness matrix can be expressed as [37]

$$\mathbf{C}^v = \mathbf{C} + i\omega\boldsymbol{\eta}. \tag{8}$$

The viscosity matrix $\boldsymbol{\eta}$, derived from the phonon viscosity tensor, has the same symmetries as the elastic matrix $\mathbf{C}$. The governing equation for a three-dimensional anisotropic linear viscoelastic medium in absence of body force is then

$$\nabla_{jI}\tilde{T}_I(\mathbf{r}) = -\rho\omega^2\tilde{u}_j, \tag{9}$$

where ∇_{jI} is the divergence operator defined by

$$\nabla_{jI} = \begin{bmatrix} \partial/\partial x & 0 & 0 & 0 & \partial/\partial z & \partial/\partial y \\ 0 & \partial/\partial y & 0 & \partial/\partial z & 0 & \partial/\partial x \\ 0 & 0 & \partial/\partial z & \partial/\partial y & \partial/\partial x & 0 \end{bmatrix}. \tag{10}$$

In this paper, we consider two-dimensional ternary viscoelastic metamaterials, as depicted in Fig. 1. The geometry parameters of the ternary metamaterial are exactly the same as those of Fig. 2(b) in Ref. [38]. The z axis is parallel to the axis of the cylindrical bars. Then if elastic waves propagate in the transverse plane (x-y plane) with displacements independent of the z coordinate, they can be decoupled into mixed and shear

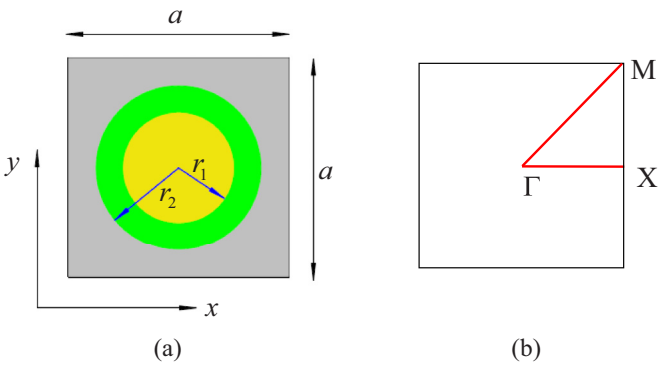

FIG. 1. (Color online) (a) Sketch of the unit cell of the square-lattice metamaterial. The inner and outer radii of the coating are r_1 and r_2, respectively. The lattice constant is a. (b) Band structures are plotted along path Γ-X-M delimiting the irreducible Brillouin zone.

modes. Accordingly, the wave equation for mixed modes is

$$\nabla\cdot(\mu^*\nabla\tilde{u}_l)+\nabla\cdot\left(\mu^*\frac{\partial}{\partial x_l}\tilde{\mathbf{u}}\right)+\frac{\partial}{\partial x_l}(\lambda^*\nabla\cdot\tilde{\mathbf{u}}) = -\rho\omega^2\tilde{u}_l,\quad l=x,y. \tag{11}$$

Here, ρ is the mass density; $\lambda^*=C_{12}^v(\mathbf{r},i\omega)$ and $\mu^*=C_{44}^v(\mathbf{r},i\omega)$ are the complex Lamé constant and the shear modulus; $\tilde{\mathbf{u}}=(\tilde{u}_x,\tilde{u}_y)$ is the displacement vector in the transverse plane; $\nabla=(\partial/\partial x,\partial/\partial y)$ is the 2D gradient operator. According to Bloch's theorem, the displacement field for eigenmodes can be expressed as

$$\tilde{u}_l(\mathbf{r})=e^{-i(\mathbf{k}\cdot\mathbf{r})}\tilde{u}_{l\mathbf{k}}(\mathbf{r}),\quad l=x,y, \tag{12}$$

where $\mathbf{r}=(x,y)$; $\mathbf{k}=(k_x,k_y)$ is the wave vector whose real part can be restricted to the first Brillouin zone of the reciprocal lattice; $\tilde{\mathbf{u}}_{l\mathbf{k}}(\mathbf{r})$ is a periodical function with the same periodicity as the crystal lattice. Substitution of Eq. (12) into Eq. (11) yields

$$(\nabla-i\mathbf{k})\cdot[\mu^*(\nabla-i\mathbf{k})\tilde{u}_{l\mathbf{k}}]+(\nabla-i\mathbf{k})\cdot[\mu^*(\nabla-i\mathbf{k})_l\tilde{\mathbf{u}}_{\mathbf{k}}] +(\nabla-i\mathbf{k})_l[\lambda^*(\nabla-i\mathbf{k})\cdot\tilde{\mathbf{u}}_{\mathbf{k}}]=-\rho\omega^2\tilde{u}_{l\mathbf{k}}, \tag{13}$$

where $\tilde{\mathbf{u}}_{\mathbf{k}}(\mathbf{r})=[\tilde{u}_{x\mathbf{k}}(\mathbf{r}),\tilde{u}_{y\mathbf{k}}(\mathbf{r})]$. Equation (13) may be rewritten in the integral form [39]

$$\int_\Omega\overline{(\nabla-i\mathbf{k})\upsilon}\cdot\mu^*(\nabla-i\mathbf{k})\tilde{u}_{l\mathbf{k}}d\mathbf{r} +\int_\Omega\overline{(\nabla-i\mathbf{k})\upsilon}\cdot\mu^*(\nabla-i\mathbf{k})_l\tilde{\mathbf{u}}_{\mathbf{k}}d\mathbf{r} +\int_\Omega\overline{(\nabla-i\mathbf{k})_l\upsilon}\cdot\lambda^*(\nabla-i\mathbf{k})\tilde{\mathbf{u}}_{\mathbf{k}}d\mathbf{r} =\omega^2\int_\Omega\rho\tilde{u}_{l\mathbf{k}}\bar{\upsilon}\,d\mathbf{r}, \tag{14}$$

where Ω is the unit cell and υ is an arbitrary periodic function in $L^2(\Omega)$.

The governing equation (13) for wave propagation in viscoelastic materials is similar to the one for elastic materials [40] and they are identical under the following replacement:

$$\lambda^*\leftrightarrow\lambda,\quad \mu^*\leftrightarrow\mu. \tag{15}$$

It is noted that λ^* and μ^* are material constants for viscoelastic materials, while λ and μ are for elastic materials. According to the elastic-viscoelastic correspondence principle for harmonic waves, the dispersion relation for the viscoelastic metamaterial can be obtained by replacing the corresponding elastic material parameters with the viscoelastic ones [41].

In Eq. (11), either $\mathbf{k}$ or ω can be considered as the real-valued independent variable [16]. In this paper, we consider time-harmonic wave propagation under a forcing frequency, and the complex band structure with complex wave numbers is obtained. The finite element method is used for calculations. Details are given in the Appendix.

III. RESULTS AND DISCUSSION

In this section, complex band structures and transmission properties of the viscoelastic metamaterial are calculated and discussed. Results for the lossless metamaterial are presented for comparison. The effective mass density of the viscoelastic metamaterial is also investigated.

A. Lossless case

1. Complex band structure

The complex band structure of the considered periodic elastic metamaterial is shown in Fig. 2. The material parameters are the same as those in Ref. [38]. The color scale in Fig. 2 represents the degree of longitudinal polarization (displacement along the x axis). For the classical band structure, it can be obtained as [42]

$$\frac{\int_S|u_x|^2dS}{\int_S(|u_x|^2+|u_y|^2)dS}=\frac{\int_S|u_{x\mathbf{k}}|^2dS}{\int_S(|u_{x\mathbf{k}}|^2+|u_{y\mathbf{k}}|^2)dS}, \tag{16}$$

where S is the whole unit cell. Values range from 0 (blue color) to 1 (red color) and measure the change in polarization from pure shear to pure longitudinal. For the complex band structure, Eq. (16) should be modified as

$$\frac{\int_S|u_{x\mathbf{k}}e^{-\mathrm{Re}(\Lambda)x}|^2dS}{\int_S(|u_{x\mathbf{k}}e^{-\mathrm{Re}(\Lambda)x}|^2+|u_{y\mathbf{k}}e^{-\mathrm{Re}(\Lambda)x}|^2)dS}, \tag{17}$$

so that the spatial decay of evanescent Bloch waves is properly included in the integrals.

Complex band structures are divided into two panels, showing the frequency as a function of the real and of the imaginary part of the wave vector. The real part of the wave vector is displayed within a range slightly exceeding the first Brillouin zone in order to highlight periodicity. In contrast, the imaginary part of the wave vector is not subjected to periodicity. It is displayed within a limited range ($|\mathrm{Im}(ka/(2\pi))|<3$), but there are other complex bands outside this range, obviously.

The classical (real-valued) band structure of Ref. [38] is displayed in Fig. 2 with the solid line for visual comparison. It can be seen that complex and classical computations give exactly the same result for real k inside the first Brillouin zone. Purely real wave numbers correspond to Bloch waves propagating without loss. However, in the real part of the complex band structure, additional modes with different dispersion are also present, that cannot be revealed by the classical

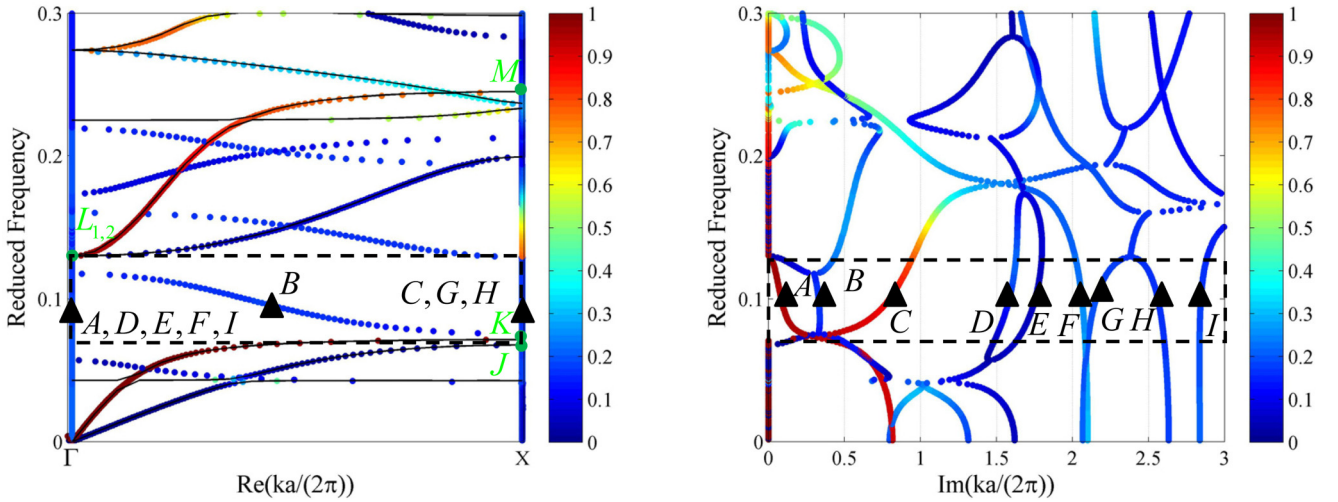

FIG. 2. (Color online) Complex band structure of the elastic metamaterial computed by FEM. The left and the right panels show the reduced frequency as a function of the real and the imaginary part of the wave vector, respectively. The solid line in the left panel is the classical (real-valued) band structure in Ref. [25]. The frequency band gap is underlined with the black dashed line.

band structure. These modes have a nonzero imaginary part of their wave vector. They are termed evanescent Bloch waves and propagate inside the PC with a spatial attenuation determined by the value of the imaginary part of the wave vector.

Because of the periodicity of the system, Bloch waves can be expanded in a series of harmonics, with each harmonic corresponding to the real part of k taken inside the first Brillouin zone and shifted by a reciprocal lattice vector. The imaginary part of k, however, is unique for each Bloch wave and determines its evanescence at a given frequency. The complex band structure shows the entire range of possible complex values of k as a function of frequency. Transmission inside a band gap is multiexponential and is dominated by the smallest nonzero value of the imaginary part of the wave vector [43], as was verified by experiment [44].

There is no physical way to excite evanescent modes in perfect (infinite) crystals because these modes do not satisfy the discrete translational symmetry [45] and they diverge as the thickness goes to infinity along the propagation direction. It is however possible to use them to explain intuitively the physics of modes inside band gaps. Furthermore, in the real world there are no infinite crystals, and any defect or edge in an otherwise perfect crystal can terminate the exponential decay and sustain evanescent modes.

Significantly, the occurrence of a band gap is not indicated by an absence of bands but by the evanescent character of Bloch waves: all Bloch waves must be evanescent within a band gap. In practice, this is a more direct and a computationally more efficient definition for a band gap, since it can be checked at an arbitrary frequency without plotting the full band structure. In the classical band structure, the number of bands at a given frequency varies. There are as many bands as degrees of freedom at low frequencies, none inside band gaps, and generally their number increases as frequency increases. In contrast, the complex band structure never misses a band, since by construction there are as many k eigenvalues as the size of the matrices, which is a constant. Complex bands are always continuous (they do not appear and disappear). Through this mechanism, the overall number of bands at any frequency is globally preserved. There is a straight connection at high symmetry points of the Brillouin zone, implying that infinite group velocity can be found in conjunction with exponential decay on propagation. The physical picture in the latter case is that of classical wave tunneling [46] in periodic structures.

Following the evolution of bands with increasing frequency, initially evanescent Bloch waves can become propagating above given cutoff frequencies. This can be understood in analogy to frustrated diffraction waves in diffraction gratings (see Refs. [47,48] for more details). As a result, it leads us to infer that the complex bands of a two-dimensional metamaterial are each associated with some diffraction order identified by a pair of indices (n_1,n_2), with n_2 defined by the modal distribution in the transverse direction. To illustrate this, we present in Fig. 3 the modal distribution at selected points of the complex band structure of Fig. 2, normalized to the maximum amplitude of the displacement in each case. For each Bloch wave, there is a dominant displacement component, in agreement with the polarization degree shown in Fig. 2. The modal distributions of the dominant component at points A–E show no oscillation in the transverse direction; they are frustrated (0, 0) diffraction orders [47]. Above the upper band gap edge of the classical band structure, the band supporting point A gets hybridized with the fifth propagating band. Other bands show similar hybridizations as the frequency increases. There is exactly one oscillation in the transverse direction at points F–H; those Bloch waves are frustrated (0, 1) diffraction orders. The modal distribution at point I lead us to associate it with frustrated (0, 2) diffraction orders. By using the dominant displacement component to define the diffraction order, it can be seen that the other component is apparently one order higher. This situation results from the connection between displacements through their derivatives in the governing equation (11). Besides, the larger the diffraction order n_2, the larger the imaginary part of the wave vector.

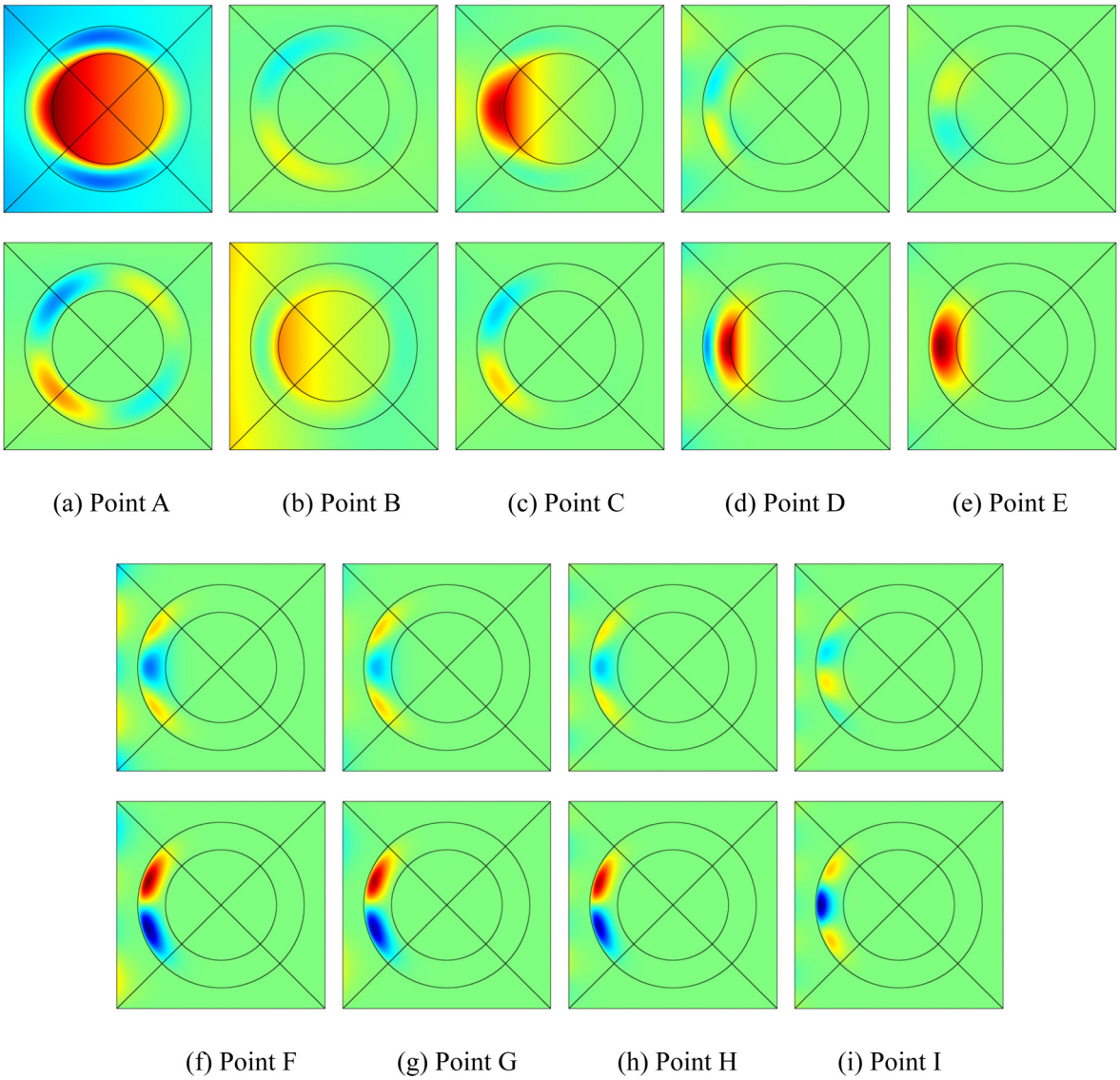

FIG. 3. (Color online) Modal distribution of the displacement component (top) u and (bottom) v at the marked points in Fig. 2. For each Bloch wave, displacements are normalized to the maximum total displacement.

Let us consider more precisely the complete band gap that is opened around reduced frequency 0.1 in Fig. 2. It was shown in Ref. [38] that this band gap is of locally resonant origin. The complex band structure shows in addition that the quasilongitudinal and the quasishear evanescent Bloch waves form quite distinct sub-band structures within it. The two quasilongitudinal LR bands with the smallest imaginary part form the characteristic shape of a cusp, a feature of the LR band gap for pressure waves described in Ref. [49]. Point A belongs to the uppermost of these two complex bands; point C belongs to the continuation of the other complex band after their crossing. In contrast, the quasishear LR sub-band structure does not form a cusp but an avoided crossing in the complex plane; point B belongs to the complex band joining two extremal points (with vanishing slope) for the imaginary part of the complex band structure. The frequency range over which the smallest imaginary part retains a significant value is larger than that for the quasilongitudinal LR case. As will be seen next, this property transfers to the width of the associated transmission dip.

2. *Transmission properties*

The transmission properties of a finite metamaterial system composed of eight unit cells were evaluated. The calculation model is shown in the inset of Fig. 4. An incident plane wave with unit amplitude is launched at the left boundary and propagates along the x direction. Periodic boundary conditions are still applied along the y direction. In this paper, transmission is defined as

$$TC = \log\left(\frac{\int |u_t|/L_0 ds}{|u_i|}\right), \tag{18}$$

where $|u_t|$ and $|u_i|(=1)$ are the amplitudes of the transmitted and incident waves, respectively; s is the right boundary with the length L_0 where the transmitted wave is recorded. As a note, transmission thus defined can exceed unity without violating energy conservation.

Transmission spectra for the metamaterial without viscosity are presented in Fig. 4. Both x- and y-polarized wave sources

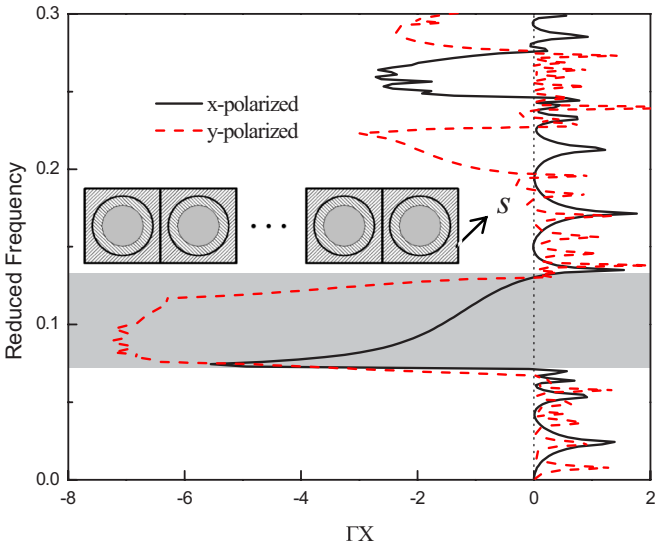

FIG. 4. (Color online) Transmission properties of the elastic metamaterial with 1×8 unit cells. The solid and dashed lines represent the x- and y-polarized wave sources, respectively. The inset shows the calculation supercell. An incoming wave with unit amplitude is incident on the left boundary, and the amplitude of the trasmitted wave is recorded on the right boundary.

are considered. It is seen that transmission is clearly attenuated inside the band gap and that the band gap width is almost the same for both sources. The shapes of the transmission curves, however, are different and are related to the variations of the smallest imaginary part of the wave vector in the complex band structure. For the x-polarized source, the transmission has a sharp minimum at the crossing point of the two longitudinal bands supporting points A and C. For the y-polarized source, the transmission dip is larger and deeper, and appears at frequencies where the imaginary parts of the dominantly transverse bands are degenerate, including point B. The attenuation of the y-polarized wave is larger than that of the x-polarized wave at all frequencies within the band gap. In the complex band structure of Fig. 2, the smallest imaginary part of the wave vector is always for the dominantly longitudinal wave, with the consequence that the displacement amplitude of the dominantly longitudinal wave decreases more slowly. The dominantly shear and dominantly longitudinal band gaps are opened starting from points J and K, respectively. The displacements distribution at these two points is shown in Fig. 5. Though they have slightly different frequencies, these two Bloch waves sitting at the X point of the first Brillouin zone clearly originate from a twice-degenerate resonance of the coated bar embedded in the matrix. The Bloch wave at point A has a definite resemblance with the dominantly longitudinal Bloch wave at point K. The Bloch wave at point B also has some resemblance with the dominantly shear Bloch wave at point J, but it extends in the matrix as much as in the central bar. The exit of both band gaps is at the degenerate points L_1 and L_2, also shown in Fig. 5 for completeness. There are also some enhanced transmission peaks at frequencies outside the complete band gap, which can be attributed to the Fabry-Pérot oscillations in the crystal [7,49].

B. Viscoelastic case

1. Viscoelastic coating

We now turn our attention to the influence of viscosity and start with the case of a viscoelastic coating. Complex

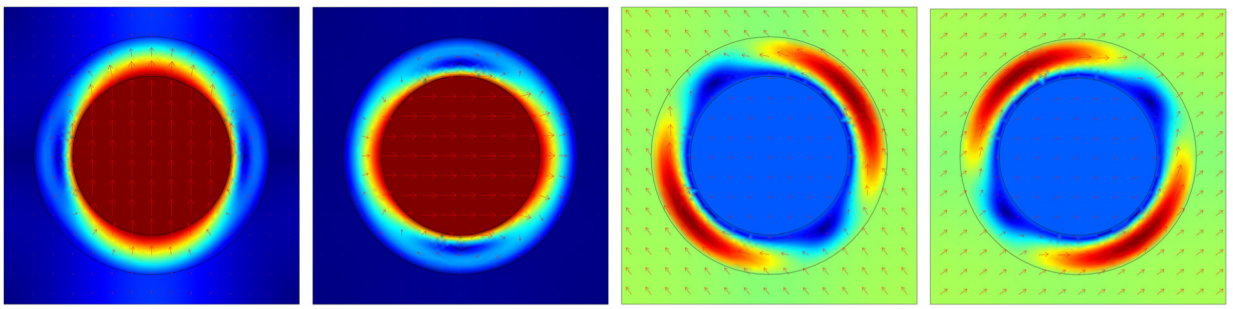

(a) Point J (b) Point K (c) Point L_1 (d) Point L_2

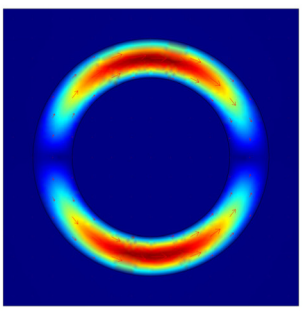

(e) Point M

FIG. 5. (Color online) Bloch waves at the marked points in Fig. 2(a). The arrows represent the amplitude and direction of vibrations.

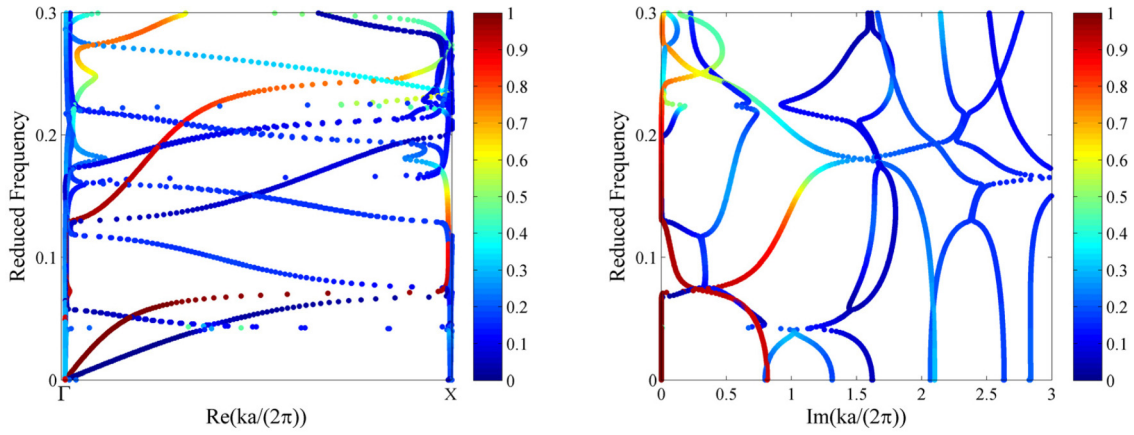

(a) $\bar{\eta}_{44}^{\text{coating}} = 4.53\times10^{-4}$

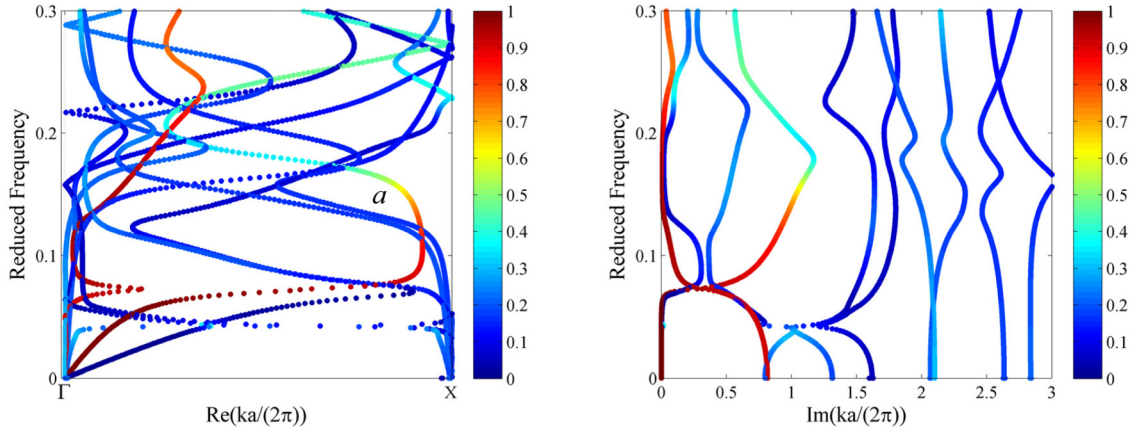

(b) $\bar{\eta}_{44}^{\text{coating}} = 6.79\times10^{-3}$

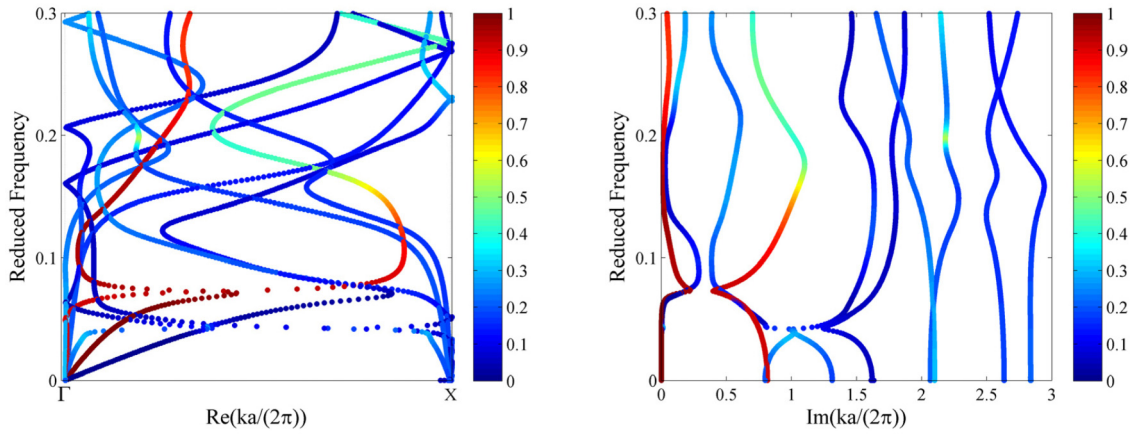

(c) $\bar{\eta}_{44}^{\text{coating}} = 1.13\times10^{-2}$

FIG. 6. (Color online) Complex band structures of lossy metamaterials with viscoelastic coating computed by FEM. The geometry parameters of the unit cell are the same as those used in Fig. 2. The viscosity of the viscoelastic coating is increased from (a) to (c).

band structures for increasing viscosity values are shown in Fig. 6. It should be noted that many different polymer or rubber compositions can be obtained experimentally, and that they can have quite different values of viscosity. The values for viscosity in this paper are arbitrary and are intended for qualitative comparison only [18]. Here the normalized viscosity $\bar{\eta}_{44} = \eta_{44}c_s/(C_{44}a)$ is used, where η_{44} is the viscosity, a is the lattice constant, and c_s and C_{44} are the transverse velocity and the shear modulus of the corresponding lossless material, respectively. When a small viscosity is considered

for the coating [Fig. 6(a) with $\bar{\eta}_{44}^{\text{coating}} = 4.53 \times 10^{-4}$], the first visible effect is the separation of initially degenerate bands, especially in the high frequency range. All sharp corners at high symmetry points of the Brillouin zone become rounded. The straight connections at high symmetry points become divergent. Compared to the lossless case of Fig. 2, it is easier to follow the evolution of complex bands. When considering a larger viscosity value [Fig. 6(b) with $\bar{\eta}_{44}^{\text{coating}} = 6.79 \times 10^{-3}$], rounding effects get more pronounced. The real wave vector of band a in Fig. 6(b) even does not occupy every value in the range [0, 0.5], so that a wave number band gap is apparent [15]. When viscosity is further increased [Fig. 6(c) with $\bar{\eta}_{44}^{\text{coating}} = 1.13 \times 10^{-2}$], the wave number band gap is enlarged. It is also interesting to observe that the addition of viscosity can break the continuity of complex bands, as predicted theoretically in Ref. [20]. For example, the two bands supporting points A and C are crossing in the lossless case. When a large viscosity value is introduced, these bands are reshaped and are avoiding each other.

The rounding of sharp corners of the complex band structure at high symmetry points was precisely described by considering the transformation of implicit dispersion relations in presence of loss [20]. Let us outline here a simple alternative explanation inspired by the case of photonic crystals [45]. Examining bands in the immediate vicinity of the gap in the lossless case, let us try to approximate the first band near the gap by expanding $\omega(k)$ in powers of complex k about the zone edge $k_0 = \pi/a$ (X point of the first Brillouin zone) or $k_0 = 0$ (Γ point of the first Brillouin zone) via a Taylor expansion [45]. Because of time-reversal symmetry, the expansion cannot

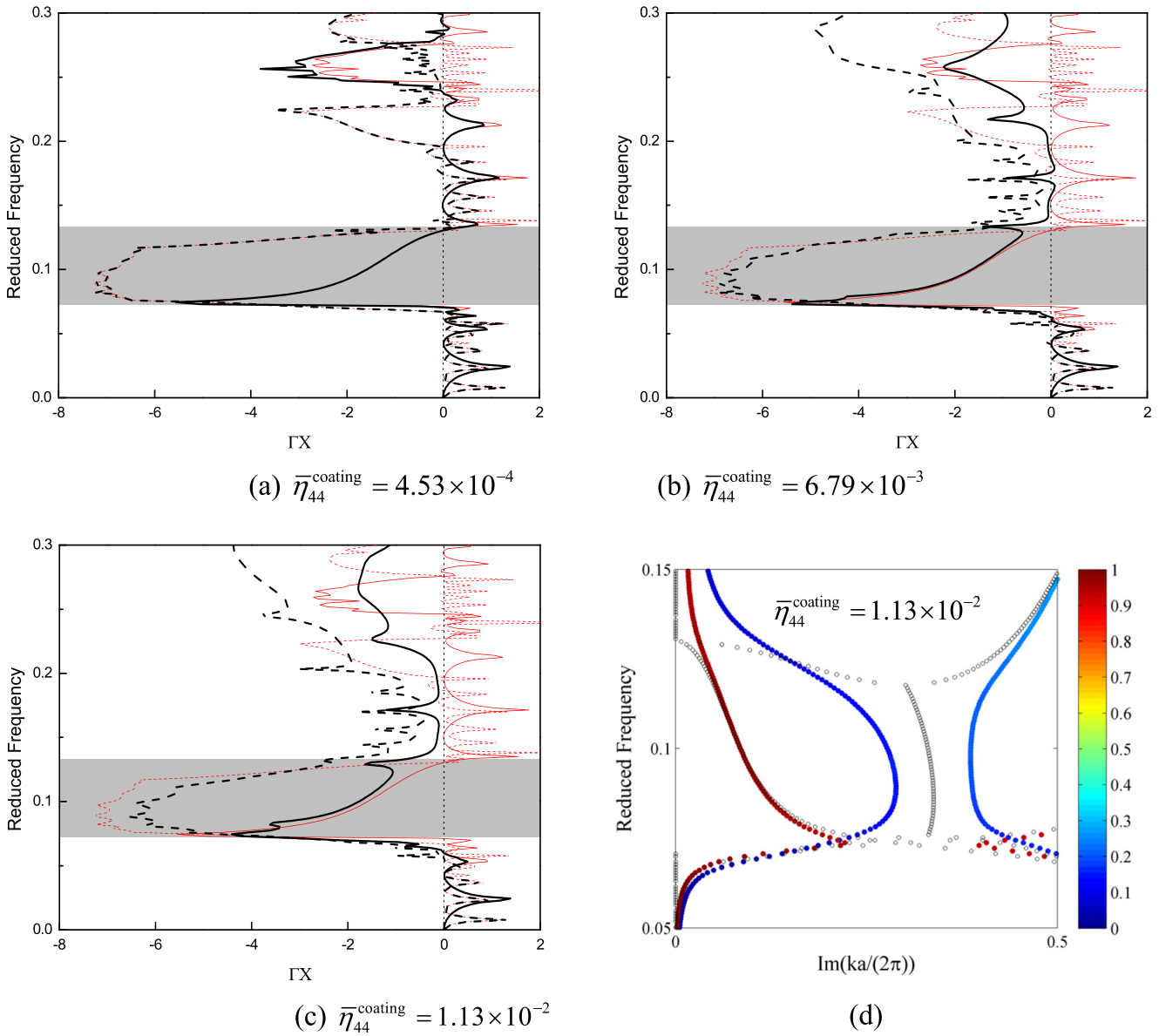

FIG. 7. (Color online) Transmission properties of a metamaterial with viscoelastic coating with increasing viscosity values from (a) to (c), shown with thick lines. The results of the elastic metamaterial (no viscosity) in Fig. 4 are shown with thin lines. Panel (d) shows the zoomed complex band structure for the viscoelastic coating with $\bar{\eta}_{44}^{\text{coating}} = 1.13 \times 10^{-2}$. Open circles represent the results for the elastic coating.

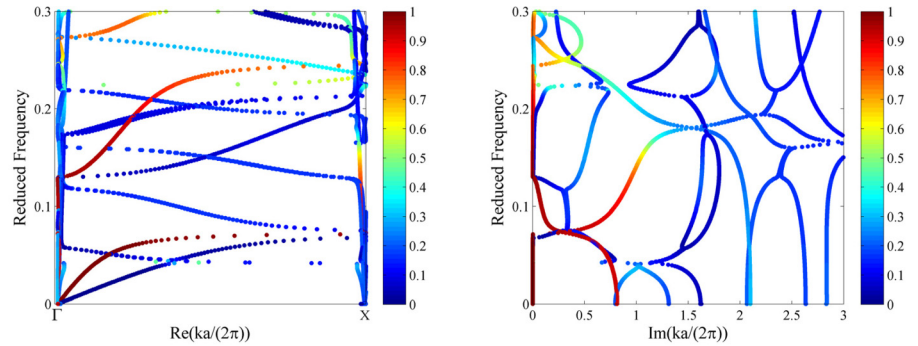

(a) $\overline{\eta}_{44}^{\text{matrix}} = 5.61\times10^{-2}$

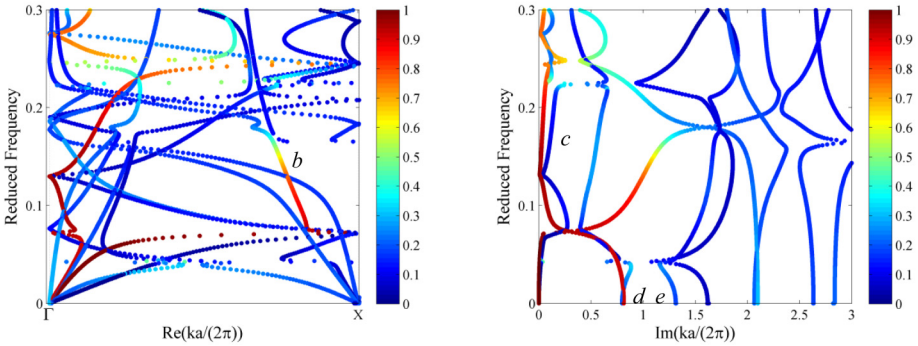

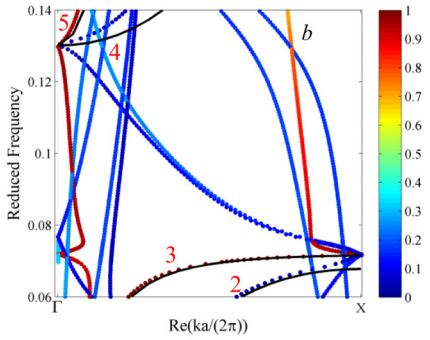

(b) $\overline{\eta}_{44}^{\text{matrix}} = 1.12$

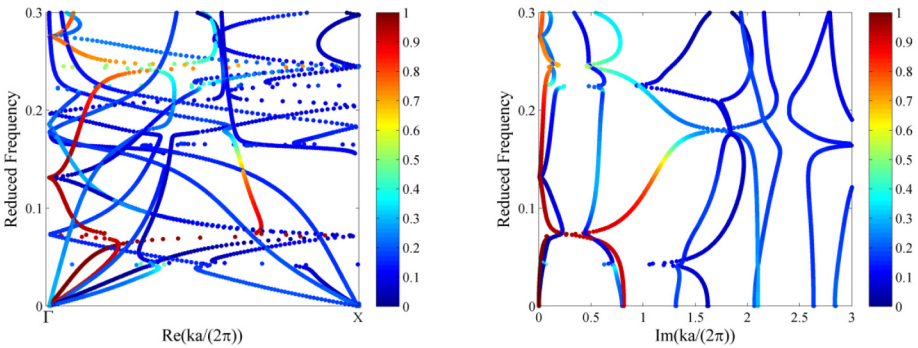

(c) $\overline{\eta}_{44}^{\text{matrix}} = 2.81$

FIG. 8. (Color online) Complex band structures of lossy metamaterials with viscoelastic matrix computed by FEM. The geometry parameters of the unit cell are the same as those used in Fig. 2. The viscosity of the viscoelastic matrix is increased from (a) to (c).

contain odd powers of k, so to lowest order,

$$\Delta\omega = \omega(k) - \omega(k_0) \approx \zeta(k-k_0)^2 = \zeta(\Delta k)^2 = \zeta(f+gi)^2, \tag{19}$$

where ζ is a constant related to the second derivative of the band. For $\Delta\omega > 0$ and for the lossless case, we are within the gap and Δk is purely imaginary ($f = 0, g \neq 0$). For the same $\Delta\omega > 0$ and for the lossy case, g becomes either larger or smaller. A nonzero f is however needed to satisfy Eq. (19). Thus the real part of the wave vector inside the irreducible Brillouin zone gets either smaller or larger but changes continuously in any case and results in a rounding of the band.

Transmission curves for the metamaterial with viscoelastic coating are shown in Fig. 7. When a small viscosity is introduced [Fig. 7(a)], transmission peaks become smooth, especially at high frequencies. Meanwhile, transmission inside the band gap is almost unaffected. When viscosity is increased [Figs. 7(b) and 7(c)], transmission peaks disappear completely above the band gap and are replaced by transmission dips. There is no clear upper band gap edge anymore, and the lower band gap edge apparently shifts down, following the rounding of complex bands. Transmission is generally decreased outside of the band gap. At the LR band gap frequencies, however, transmission is instead increased. This effect can be explained by the change in the complex band structure, as shown in Fig. 7(d). The separation of the originally degenerate bands results effectively in a smaller minimum imaginary part for the wave number. As a consequence, the wave decays more slowly along the propagation direction, and a larger transmission is observed at the exit of the finite metamaterial. For the longitudinal wave, the same effect is less pronounced but the reconstruction of the bands under viscosity also gives rise to a smaller minimum imaginary part of the wave number around the initial crossing point. As a result, the transmission dip is less deep as well.

2. *Viscoelastic matrix*

Complex band structures for a viscoelastic matrix with different viscosity values are presented in Fig. 8. Similar to the case of the viscoelastic coating, shown in Fig. 7(a), for a small viscosity value of the matrix [Fig. 8(a) with $\bar{\eta}_{44}^{\text{matrix}} = 5.61 \times 10^{-2}$] there is a clear influence on the real part of the bands, especially at high symmetry points, but the imaginary part remains mostly unaffected. For a larger viscosity value [Fig. 8(b) with $\bar{\eta}_{44}^{\text{matrix}} = 1.12$], the effect gets more pronounced. Some degenerate modes are separated, such as the real part of the band supporting point B and

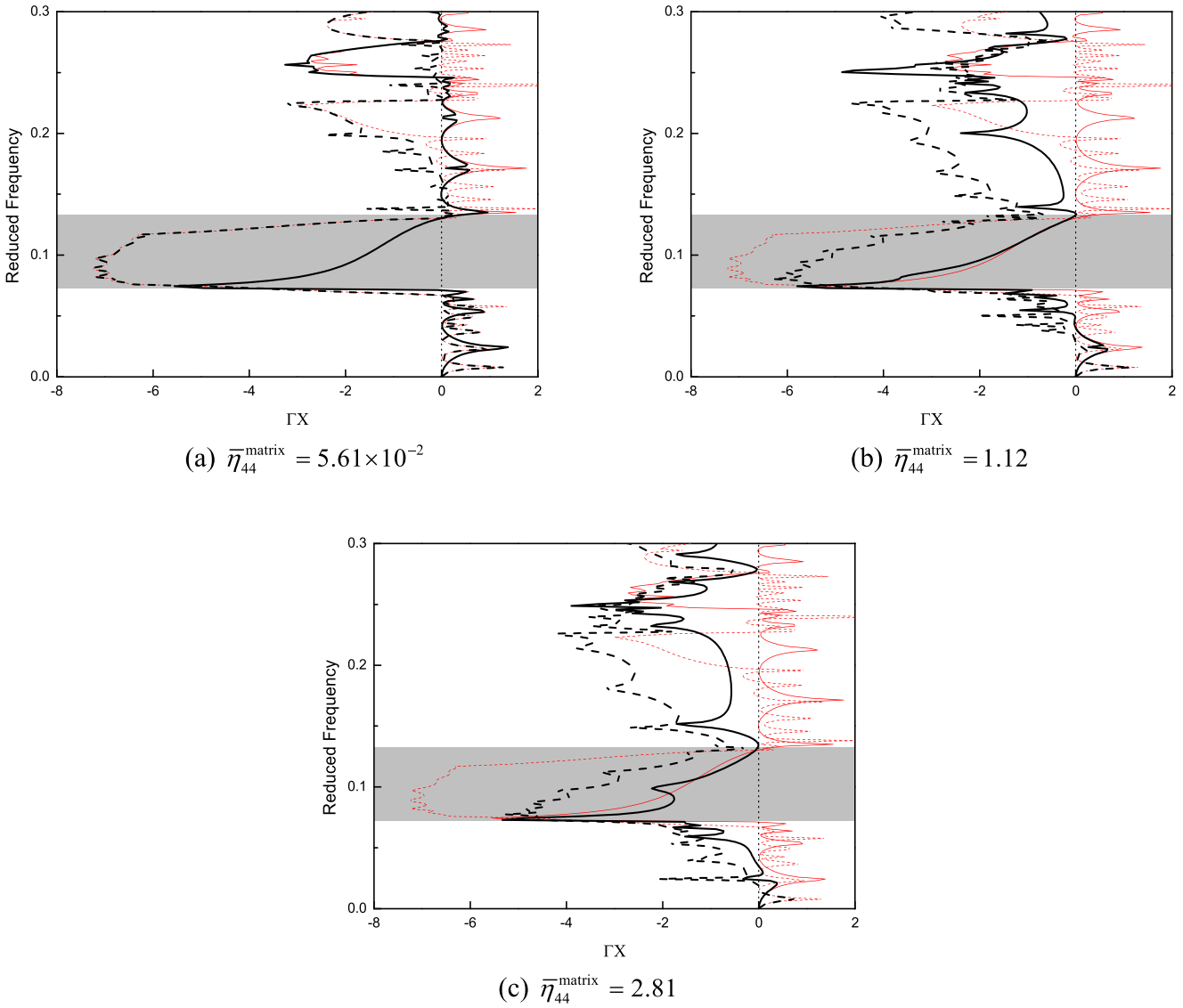

(a) $\bar{\eta}_{44}^{\text{matrix}} = 5.61 \times 10^{-2}$ (b) $\bar{\eta}_{44}^{\text{matrix}} = 1.12$

(c) $\bar{\eta}_{44}^{\text{matrix}} = 2.81$

FIG. 9. (Color online) Transmission properties of a metamaterial with viscoelastic matrix with increasing viscosity values from (a) to (c), shown with thick lines. The results of the elastic metamaterial (no viscosity) in Fig. 4 are shown with thin lines, for comparison. The third panel in (b) is a zoom of the complex band structure in the band gap range.

the imaginary part of the bands supporting points G and H in the lossless case. Viscosity has mostly a linear effect on the complex bands, where the imaginary or the real part increases or decreases linearly. For example, the real part of band b decreases linearly, while the imaginary part of band c increases linearly, as shown in Fig. 8(b). It is also noted that cusps are formed at the band gap edges of the real part of the band structure, where their first order derivatives are not continuous, which is different from the results with the viscoelastic coating. Complex bands at low frequencies are also affected: the imaginary part of band d decreases and that of band e increases. When viscosity is increased even more [Fig. 8(c) with $\bar{\eta}_{44}^{\text{matrix}} = 2.81$], the above phenomenon gets even more pronounced.

Figure 9 presents transmission spectra for the viscoelastic matrix with different viscosity values. For passing bands, the effect of viscosity is similar to the case of the viscoelastic coating. We observe again that inside the LR band gap, transmission is increased in the viscous case compared to the elastic case. The increase in transmission, moreover, is mostly linear with frequency for the y-polarized wave, which was not the case for the viscoelastic coating case in Fig. 7.

All changes in the complex band structures and in transmission spectra are a result of the dispersive and dissipative effects of viscosity. The effect of dispersion is chiefly to displace bands in the complex plane; sharp corners become rounded and initially propagating waves become evanescent. The effect of dissipation is to enhance attenuation in passing bands but to enhance transmission in LR band gap ranges. It is expected that transmission should be decreased in passing bands when viscosity is introduced, because viscosity then implies attenuation on propagation just as in homogeneous media. Viscosity also decreases transmission inside Bragg band gaps [7], in accordance with the transformation of the complex band structure [18]. In contrast, the opposite effect of viscosity at the transmission dip caused by a local resonance is less intuitive. We think that viscosity damps the local resonators, making the physical mechanism creating the dip less efficient, because the resonators are less prone to storing the incident energy. Though the phenomenon is certainly captured by the complex band structure, providing a complete physical explanation remains a challenge for future work.

C. Effective mass density

Here we use FEM [28–31] to calculate the effective mass density of the viscoelastic metamaterial. The four boundaries of the unit cell are assumed to be subjected to a global displacement u_i. In the study, displacement phase differences among the four boundaries of the unit cell are ignored according to the long wavelength assumption. Therefore, the effective mass density of the unit cell can be determined through the averaged reaction force at the boundary nodes, and is given by

$$\rho_{ij}^{\text{eff}} = F_i / \ddot{U}_j, \tag{20}$$

where $F_i = S^{-1} \int_{\partial S} \sigma_{ij} n_j dl$ is the averaged resultant force on the boundaries and $\ddot{U}_i = L^{-1} \int_{\partial S} \ddot{u}_i dl$ is the averaged acceleration; $i, j = 1,2$, σ_{ij}, u_i, and $\ddot{u}_i$ are the local stress, displacement, and acceleration fields, respectively; n_i denotes the unit vector normal to the boundary; S and ∂S denote the area and external boundary with length L of the unit cell. Anisotropic mass density may appear for metamaterials with symmetries other than the square and hexagonal symmetry [24] or for an elastic metamaterial when rotating an elliptical coating [29]. For the circular coating with high symmetry considered in this paper, we have an isotropic effective mass density, i.e., $\rho_{11}^{\text{eff}} = \rho_{22}^{\text{eff}}$ and $\rho_{12}^{\text{eff}} = \rho_{21}^{\text{eff}} = 0$.

The effective mass density of the lossless metamaterial is shown as a function of frequency in Fig. 10 with the thin solid line. Two NMD regions are observed, i.e., $0.07 < \Omega < 0.131$ and $0.244 < \Omega < 0.274$, corresponding to the dipolar

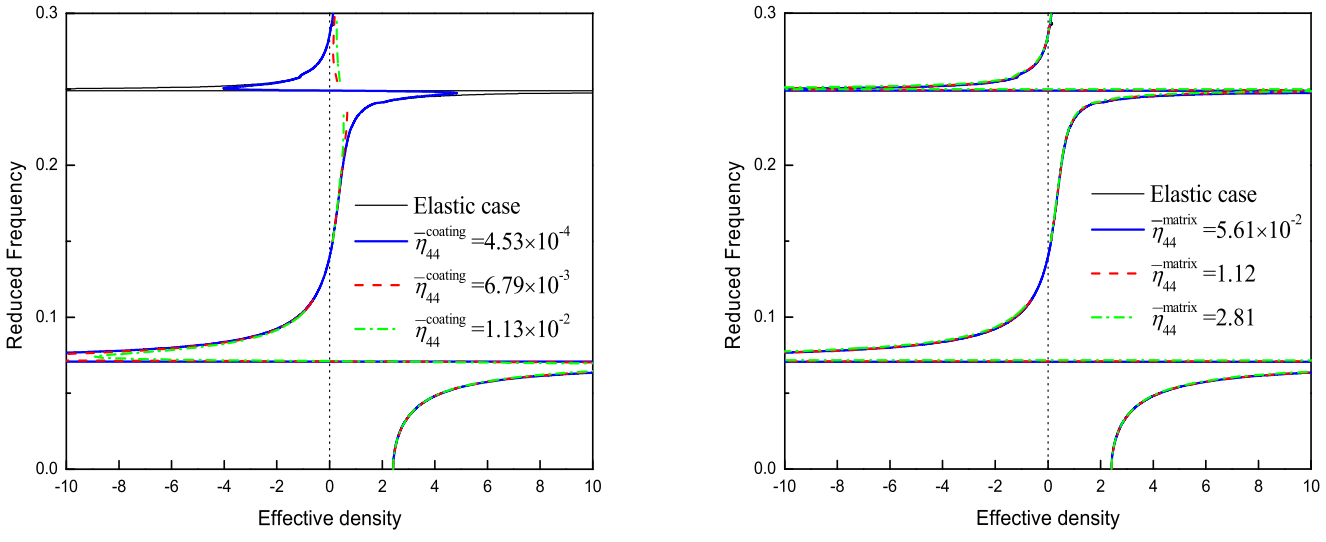

(a) Viscoelastic coating (b) Viscoelastic matrix

FIG. 10. (Color online) Effective mass density of the metamaterial with viscoelastic (a) coating and (b) matrix calculated by FEM. Results are normalized to the mass density of the elastic matrix.

resonances of the core and of the coating, respectively; see the vibration modes in Figs. 5(b) and 5(e). For the viscoelastic coating in Fig. 10(a), the viscosity value has little effect on the NMD region at low frequencies, but has some influence on the value of the NMD. In contrast, it has a strong influence on the NMD region at high frequencies, corresponding to local vibration of the coating in Fig. 5(e). A larger viscosity value ($\bar{\eta}_{44}^{\text{coating}} = 1.13 \times 10^{-2}$) for the coating can even result in the disappearance of this region.

Contrary to the case of the viscoelastic coating, the viscosity of the matrix has almost no influence on the two NMD regions, but has little influence on the value of the NMD, as apparent in Fig. 10(b), because these two NMD regions are generated by the local vibration of the inner core or of the coating, while the matrix almost stands still.

The NMD can also be evaluated by the Lorentz model [32]:

$$\rho_{\text{eff}} = S^{-1}\left(m_2 + \frac{m_1\bar{K}}{\bar{K} - m_1\omega^2}\right) = S^{-1}\pi(C_{44} + i\omega_2\eta_{44}) \times \frac{r_1(2-2\nu)/(1-2\nu) + r_2}{r_2 - r_1}, \tag{21}$$

where the effective stiffness,

$$\bar{K} = \frac{\pi(r_1C_{11} + r_2C_{44})}{r_2 - r_1} = \frac{(r_1(2-2\nu)/(1-2\nu) + r_2)}{r_2 - r_1}\pi C_{44}, \tag{22}$$

is obtained by Eq. (5) in Ref. [38]. Here only the viscoelastic coating is considered, because the matrix has no contribution to the effective stiffness $\bar{K}$ in the model.

Figure 11 shows the effective mass density calculated using the Lorentz model. The result is in good agreement with the FEM result in Fig. 10(a) for the low frequency resonance. However, the Lorentz model fails to predict the NMD region at high frequencies, because the corresponding vibration locates in the coating which is considered to be solely a spring in the model.

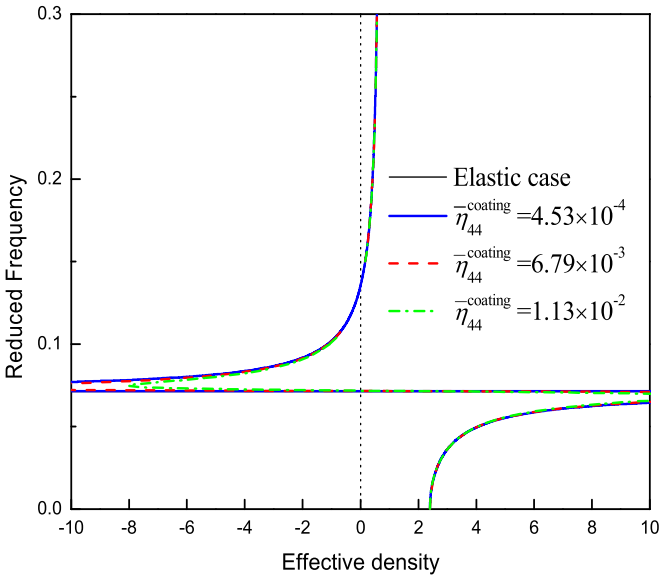

FIG. 11. (Color online) Effective mass density of the metamaterial with viscoelastic coating as predicted by using Lorentz's model. Results are normalized to the mass density of the elastic matrix.

IV. CONCLUDING REMARKS

Wave propagation in two-dimensional viscoelastic metamaterials has been investigated. An algorithm for calculating the complex band structure for in-plane waves was developed based on a FEM implementation. Propagating and evanescent Bloch waves were calculated and analyzed in order to understand the physical meaning of the associated complex bands. Viscosity was considered for either the matrix or the coating. Its effect on the complex band structure of the infinite metamaterial and on the transmission properties through a finite piece of metamaterial was examined. The effective mass density was also studied. From the calculated results and discussions we can draw the following conclusions.

(1) The proposed method provides an exact result for the complex band structure, the real part of which is the same as the classical band structure. Complex bands are associated with diffraction orders determined by the modal distribution of the dominant displacement component, while the other displacement is one order higher.

(2) When viscosity is introduced, the degeneracy of bands in the elastic case is lifted, and the sharp corners at high symmetry points of the Brillouin zone become rounded.

(3) In the passing bands, the transmission of a finite but viscoelastic metamaterial gets worsened. In contrast, inside locally resonant band gaps the transmission around the dip frequency is enhanced due to the separation of initially degenerate complex bands. The lower band gap edge shifts down, while the upper edge eventually becomes fuzzy. All changes in the complex band structures and in transmission spectra are a result of the dispersive and dissipative effects of the viscosity.

(4) Compared to viscosity of the matrix, viscosity of the coating has a stronger influence on the effective mass density, especially at high symmetry points. Furthermore, viscosity of the coating can increase the magnitude of the negative mass density, and even result in its disappearance for a resonance localized in the coating.

ACKNOWLEDGMENTS

The first two authors are grateful for the support from National Natural Science Foundation of China (Grant No. 11532001). The third author acknowledges the financial support by the Labex ACTION program (Contract No. ANR-11-LABX-01-01).

APPENDIX

In this appendix, we detail the calculation process of the complex band structure by using the commercial software Comsol Multiphysics. Due to the periodicity of the PCs, the calculation is implemented in a representative unit cell. Periodic boundary conditions based on the Bloch's theorem Eq. (12) are applied to relate the two opposite boundaries of the unit cell. The unit cell is meshed by using a quadrilateral mesh with Lagrange quadratic elements. Eigenfrequency analysis is

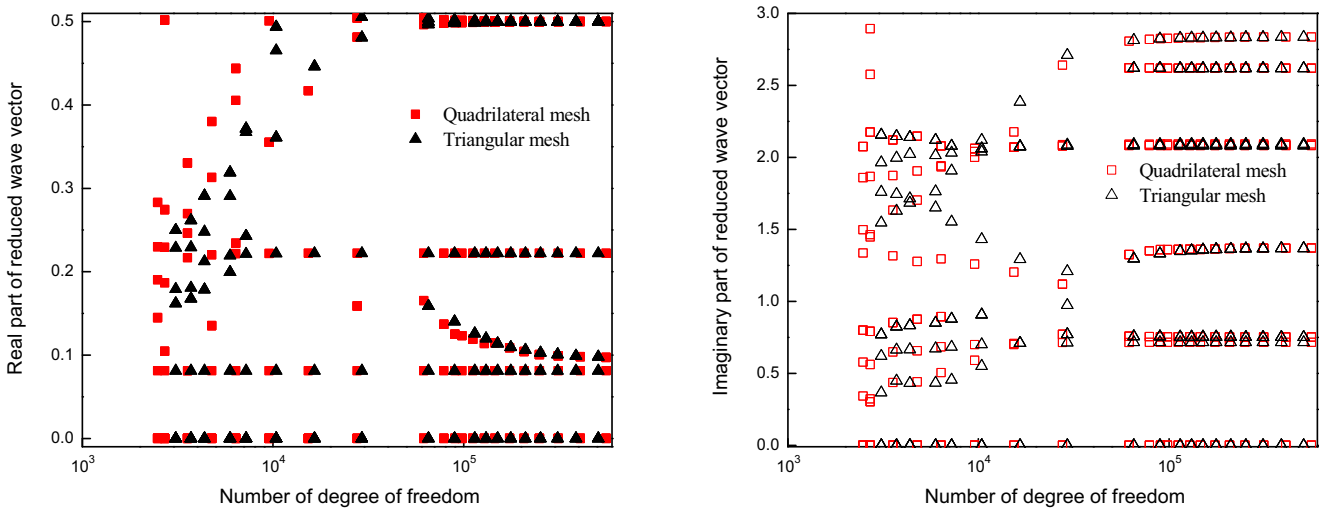

FIG. 12. (Color online) Convergence of the complex bands calculated by FEM with triangular and quadrilateral elements at the reduced frequency $\Omega = 0.05$. The real (imaginary) part of the wave vector is shown in the left (right) panel.

performed and SPOOLES [50] is selected as the linear system solver. The frequency ω is swept in the desired frequency range, so as to obtain the complex band structure. In practice for the figures of this paper, 450 frequency points are selected and 240 eigenvalues are solved for each frequency.

Numerical calculations are implemented by utilizing the *PDE (Partial Difference Equation) module* of Comsol. The *PDE module* is an application mode for equation-based modeling, and *Coefficient form* is for linear or almost linear PDE formulations. With two independent variables, the PDE problem in coefficient form results in the following eigenvalue equation system:

$$e_a \Lambda^2 \mathbf{U} - d_a \Lambda \mathbf{U} - \nabla \cdot (c : \nabla \mathbf{U} + \alpha \mathbf{U} - \gamma) + b\mathbf{U} + \beta \cdot \nabla \mathbf{U} = f \text{ in } \Omega, \tag{A1}$$

To obtain an eigenvalue problem for $k(\omega)$, we write $\mathbf{k} = k\boldsymbol{\theta}$ [34], where k is the amplitude of the wave vector along the propagation direction at a given frequency, and $\boldsymbol{\theta} = (\cos\theta, \sin\theta)$ is a unit direction vector along the elastic wave propagation. The eigenvalue is set to be $\Lambda(k) = -ik$. By comparing Eq. (13) with Eq. (A1), the nonzero coefficients in Eq. (A1) are obtained, i.e.,

$$c = \begin{pmatrix} \begin{pmatrix} (\lambda+2\mu) & 0 \\ 0 & \mu \end{pmatrix} & \begin{pmatrix} 0 & \lambda \\ \mu & 0 \end{pmatrix} \\ \begin{pmatrix} 0 & \mu \\ \lambda & 0 \end{pmatrix} & \begin{pmatrix} \mu & 0 \\ 0 & (\lambda+2\mu) \end{pmatrix} \end{pmatrix}, \tag{A2a}$$

$$e_a = \begin{pmatrix} -(\lambda+2\mu)\cos^2\theta - \mu\sin^2\theta & -(\lambda+\mu)\sin\theta\cos\theta \\ -(\lambda+\mu)\sin\theta\cos\theta & -\mu\cos^2\theta - (\lambda+2\mu)\sin^2\theta \end{pmatrix}, \tag{A2b}$$

$$\alpha = \begin{pmatrix} \begin{pmatrix} (\lambda+2\mu)\Lambda\cos\theta \\ \mu\Lambda\sin\theta \end{pmatrix} & \begin{pmatrix} \lambda\Lambda\sin\theta \\ \mu\Lambda\cos\theta \end{pmatrix} \\ \begin{pmatrix} \mu\Lambda\sin\theta \\ \lambda\Lambda\cos\theta \end{pmatrix} & \begin{pmatrix} \mu\Lambda\cos\theta \\ (\lambda+2\mu)\Lambda\sin\theta \end{pmatrix} \end{pmatrix}, \tag{A2c}$$

$$\beta = \begin{pmatrix} (-(\lambda+2\mu)\Lambda\cos\theta & -\mu\Lambda\sin\theta) & (-\mu\Lambda\sin\theta & -\lambda\Lambda\cos\theta) \\ (-\lambda\Lambda\sin\theta & -\mu\Lambda\cos\theta) & (-\mu\Lambda\cos\theta & -(\lambda+2\mu)\Lambda\sin\theta) \end{pmatrix}, \tag{A2d}$$

$$b = \begin{pmatrix} -\rho\omega^2 & 0 \\ 0 & -\rho\omega^2 \end{pmatrix}. \tag{A2e}$$

The quadratic eigenvalue problem of Eq. (A1) is next reformulated as a linear eigenvalue problem by the following transformation:

$$\mathbf{V} = \Lambda\mathbf{U}, \quad e_a \Lambda \mathbf{V} - \nabla \cdot (c : \nabla \mathbf{U} + \alpha \mathbf{U}) + b\mathbf{U} + \beta \cdot \nabla \mathbf{U} = 0. \tag{A3}$$

After constraint handling, it is possible to write the system in the form $Ax = \Lambda Bx$. Finding the eigenvalues is equivalent to computing the largest eigenvalues of the matrix

$$C = A^{-1}B. \tag{A4}$$

To do this, the solver uses the ARPACK Fortran routines for large-scale eigenvalue problems [51]. C is a skew-symmetric matrix in the elastic case, and the obtained eigenvalues are quadruples $(\Lambda, -\Lambda, \bar{\Lambda}, -\bar{\Lambda})$, with $\bar{\Lambda}$ being the complex conjugate of Λ. In the viscoelastic case, the obtained eigenvalues are couples $(\Lambda, -\Lambda)$.

It is also noted that since C in Eq. (A4) is skew-symmetric in the elastic case, a large number of degree of freedom is needed to get a convergent result. It is expected that this property remains true in the viscoelastic case, by continuity. Convergence of the complex bands calculated using triangular and quadrilateral elements is compared in Fig. 12 at $\Omega = 0.05$. The convergence for the triangular mesh is a little worse than that of the quadrilateral mesh. The results converge when the number of the degree of freedom is about 3×10^5, which is about two orders higher than the results of the real band structure in Ref. [38].

[1] M. S. Kushwaha, P. Halevi, L. Dobrzynski, and B. Djafari-Rouhani, Phys. Rev. Lett. **71**, 2022 (1993).
[2] Z. Y. Liu, X. X. Zhang, Y. W. Mao, Y. Y. Zhu, Z. Y. Yang, C. T. Chan, and P. Sheng, Science **289**, 1734 (2000).
[3] M. I. Hussein, M. J. Leamy, and M. Ruzzene, Appl. Mech. Rev. **66**, 040802 (2014).
[4] D. J. Mead, J. Sound Vib. **27**, 235 (1973).
[5] B. Merheb, P. A. Deymier, K. Muralidharan, J. Bucay, M. Jain, M. Aloshyna-Lesuffleur, R. W. Greger, S. Mohanty, and A. Berker, Modell. Simul. Mater. Sci. Eng. **17**, 075013 (2009).
[6] I. E. Psarobas, Phys. Rev. B **64**, 012303 (2001).
[7] Y. Z. Liu, D. L. Yu, H. G. Zhao, J. H. Wen, and X. S. Wen, J. Phys. D: Appl. Phys. **41**, 065503 (2008).
[8] J. H. Oh, Y. J. Kim, and Y. Y. Kim, J. Appl. Phys. **113**, 106101 (2013).
[9] S. Mukherjee and E. H. Lee, Comput. Struct. **5**, 279 (1975).
[10] R. Sprik and G. H. Wegdam, Solid State Commun. **106**, 77 (1998).
[11] X. Zhang, Z. Y. Liu, J. Mei, and Y. Y. Liu, J. Phys.: Condens. Matter **15**, 8207 (2003).
[12] Y. P. Zhao and P. J. Wei, Comput. Mater. Sci. **46**, 603 (2009).
[13] P. J. Wei and Y. P. Zhao, Mech. Adv. Mater. Struct. **17**, 383 (2010).
[14] M. I. Hussein, Phys. Rev. B **80**, 212301 (2009).
[15] M. I. Hussein and M. J. Frazier, J. Appl. Phys. **108**, 093506 (2010).
[16] T. Suzuki and P. K. L. Yu, J. Mech. Phys. Solids **46**, 115 (1997).
[17] J. D. Achenbach, *Wave Propagation in Elastic Solids* (North-Holland, Amsterdam, 1973).
[18] R. P. Moiseyenko and V. Laude, Phys. Rev. B **83**, 064301 (2011).
[19] M. Collet, M. Ouisse, M. Ruzzene, and M. N. Ichchou, Int. J. Solids Struct. **48**, 2837 (2011).
[20] V. Laude, J. M. Escalante, and A. Martinez, Phys. Rev. B **88**, 224302 (2013).
[21] E. Andreassen and J. S. Jensen, J. Vib. Acoust. **135**, 041015 (2013).
[22] J. Mei, Z. Y. Liu, W. J. Wen, and P. Sheng, Phys. Rev. Lett. **96**, 024301 (2006).
[23] J. Mei, Z. Y. Liu, W. J. Wen, and P. Sheng, Phys. Rev. B **76**, 134205 (2006).
[24] D. Torrent and J. Sanchez-Dehesa, New J. Phys. **10**, 023004 (2008).
[25] J. Mei, Y. Wu, and Z. Y. Liu, Europhys. Lett. **98**, 54001 (2012).
[26] Y. Wu, Y. Lai, and Z. Q. Zhang, Phys. Rev. B **76**, 205313 (2007).
[27] X. M. Zhou and G. K. Hu, Phys. Rev. B **79**, 195109 (2009).
[28] X. N. Liu, G. K. Hu, G. L. Huang, and C. T. Sun, Appl. Phys. Lett. **98**, 251907 (2011).
[29] A. P. Liu, R. Zhu, X. N. Liu, G. K. Hu, and G. L. Huang, Wave Motion **49**, 411 (2012).
[30] R. Zhu, X. N. Liu, G. L. Huang, H. H. Huang, and C. T. Sun, Phys. Rev. B **86**, 144307 (2012).
[31] R. Zhu, X. N. Liu, G. K. Hu, C. T. Sun, and G. L. Huang, Nat. Commun. **5**, 5510 (2014).
[32] J. R. Willis and G. W. Milton, Proc. R. Soc. A **463**, 855 (2007).
[33] H. H. Huang, C. T. Sun, and G. L. Huang, Int. J. Eng. Sci. **47**, 610 (2009).
[34] Y. Q. Liu, X. Y. Su, and C. T. Sun, J. Mech. Phys. Solids **74**, 158 (2015).
[35] A. Nougaoui and B. Djafari-Rouhani, Surf. Sci. **199**, 623 (1988).
[36] J. M. Carcione and F. Cavallini, Mech. Mater. **19**, 311 (1995).
[37] B. A. Auld, *Acoustic Fields and Waves in Solids* (John Wiley & Sons, New York, 1991).
[38] Y. F. Wang, Y. S. Wang, and L. Wang, J. Phys. D: Appl. Phys. **47**, 015502 (2014).
[39] M. I. Hussein, Proc. R. Soc. A **465**, 2825 (2009).
[40] Z. Z. Yan and Y. S. Wang, Phys. Rev. B **74**, 224303 (2006).
[41] J. M. Carcione, D. Kosloff, and R. Kosloff, Geophys. J. **93**, 393 (1998).
[42] Y. F. Wang, Y. S. Wang, and Ch. Zhang, J. Phys. D: Appl. Phys. **47**, 485102 (2014).
[43] X. Y. Ao and C. T. Chan, Phys. Rev. B **80**, 235118 (2009).
[44] V. Romero-Garcia, J. V. Sanchez-Perez, S. Castineira-Ibanez, and L. M. Garcia-Raffi, Appl. Phys. Lett. **96**, 124102 (2010).
[45] J. D. Joannopoulos, S. G. Johnson, J. N. Winn, and R. D. Meade, *Photonic Crystals: Modeling the Flow of Light*, 2nd ed. (Princeton University Press, Princeton, NJ, 2008).
[46] S. X. Yang, J. H. Page, Z. Y. Liu, M. L. Cowan, C. T. Chan, and P. Sheng, Phys. Rev. Lett. **88**, 104301 (2002).
[47] V. Laude, Y. Achaoui, S. Benchabane, and A. Khelif, Phys. Rev. B **80**, 092301 (2009).
[48] V. Laude, *Phononic Crystals* (De Gruyter, Berlin, 2015).
[49] Y. F. Wang, V. Laude, and Y. S. Wang, J. Phys. D: Appl. Phys. **47**, 475502 (2014).
[50] C. Ashcraft and R. G. Grimes, SPOOLES: An object oriented sparse matrix library, in Proceedings of the Ninth SIAM Conference on Parallel Processing for Scientific Computing, 1999, San Antonio, TX. Available online at http://www.netlib.org/linalg/spooles.
[51] R. B. Lehoucq, D. Sorensen, and C. Yang, *ARPACK Users' Guide: Solution of Large-Scale Eigenvalue Problems with Implicitly Restarted Arnoldi Methods* (SIAM, Philadelphia, 1998).